Generation of a mid-infrared broadband polarized supercontinuum in As_2Se_3 photonic crystal fibers*

Wang Xiao-Yan(王晓琰), Li Shu-Guang(李曙光)†, Liu Shuo(刘 硕), Yin Guo-Bing(尹国冰), and Li Jian-She(李建设)

Key Laboratory of Metastable Materials Science and Technology, College of Science, Yanshan University, Qinhuangdao 066004, China

(Received 10 September 2011; revised manuscript received 6 December 2011)

A simplified structure of birefringent chalcogenide As_2Se_3 photonic crystal fiber (PCF) is designed. Properties of birefringence, polarization extinction ratio, chromatic dispersion, nonlinear coefficient, and transmission are studied by using the multipole method, the finite-difference beam propagation method, and the adaptive split-step Fourier method. Considering that the zero dispersion wavelength of our proposed fiber is about 4 μm, we have analysed the mechanism of spectral broadening in PCFs with different pitches in detail, with femtosecond pulses at a wavelength of 4 μm as the pump pulses. Especially, mid-infrared broadband polarized supercontinuums are obtained in a 3-cm PCF with an optimal pitch of 2 μm. Their spectral width at −20 dB reaches up to 12 μm. In the birefringent PCF, we find that the supercontinuum generation changes with the pump alignment angle. Research results show that no coupling between eigenpolarization modes are observed at the maximum average power (i.e., 37 mW), which indicates that the polarization state is well maintained.

Keywords: polarization maintaining, photonic crystal fiber, mid-infrared supercontinuum

PACS: 42.81.Gs, 95.85.Hp, 42.65.–k, 42.62.Fi **DOI:** 10.1088/1674-1056/21/5/054220

1. Introduction

Sources of broadband mid-infrared (mid-IR) light have attracted considerable attention from many researchers due to the enormous potential applications in optical frequency metrology,[1] spectroscopy astronomy, optical tomography,[2] and infrared imagery. At present, the generation of mid-IR sources is typically based on optical parametric oscillators (OPOs) or quantum cascaded lasers (QCLs). However, wavelengths of OPOs and QCLs need to be continuously tuned to cover the entire spectral range needed. While a supercontinuum source can cover a wider spectral range without the time delay caused by the wavelength tuning of conventional sources. It is, therefore, essential to create practical, robust, and low-cost mid-IR sources for the future.

Photonic crystal fibers (PCFs) are particularly attractive candidates for supercontinuum generation (SCG) in the mid-IR region, which require law-cost materials in the wavelength range of interest, as well as appropriate nonlinear and dispersion characteristics. Above a wavelength of 2 μm, due to the loss of silica, non-silica "compound" glass PCFs (e.g., fluoride,[3,4] bismuth oxide-based,[5] tellurite,[6−8] and chalcogenide fibers[9]) have been proposed to generate broader mid-IR supercontinuum.

Compared with all other non-silica glasses, chalcogenide glasses, in particular As_2Se_3 and As_2S_3, have a larger refractive index and a higher nonlinear index, leading to a greater modal confinement and a higher nonlinearity. Moreover, they are transparent at a mid-IR wavelength of ~ 10 μm, especially for As_2Se_3 up to 14 μm. Yeom *et al.*[10] reported low-threshold mid-IR SCG in chalcogenide nanowires; Brandon *et al.*[11] obtained an output spectrum of 2.1–3.2 μm in an As_2Se_3 chalcogenide PCF using a 100-fs 2500-nm pump pulse; Hu *et al.*[12,13] optimized the bandwith of mid-IR supercontinuum sources in As_2S_3 and As_2Se_3 chalcogenide PCFs. Recently, an As_2Se_3 micro-porous fiber has been studied.[14]

Moreover, the polarization effect is another essential aspect of the SCG dynamics in PCFs. The high birefringent fibers for SCG can keep polarization states along the propagation direction for all spectral

*Project supported by the National Natural Science Foundation of China (Grant Nos. 61178026 and 60978028), the Specialized Research Fund for the Doctoral Program of Higher Education, China (Grant No. 20091333110010), and the Natural Science Foundation of Hebei Province, China (Grant No. F2009000481).

†Corresponding author. E-mail: shuguangli@ysu.edu.cn

© 2012 Chinese Physical Society and IOP Publishing Ltd

components. Many studies have been carried out on this subject, particularly in Refs. [15]–[17], where SCG in birefringent PCFs has been investigated both theoretically and experimentally. However, SCG in polarized chalcogenide PCFs has rarely been reported. In this paper, a high birefringent nonlinear As_2Se_3 PCF is designed. By modulating the fiber geometry, optimized supercontinuum sources have been obtained with an input pump pulse at a wavelength of 4.0 μm.

2. Geometry and properties of PCFs

The PCFs have been demonstrated to be one of the most appropriate structures for the enhancement of polarization effect because of various possibilities of geometry variation. In Fig. 1, the cross section and fundamental mode field distribution of the birefringence PCF we proposed are illustrated. The PCF is composed of a series of air holes arranged in an isosceles triangle lattice, and the background material is chalcogenide (As_2Se_3) glass. In addition, four air holes arranged in an rhombus array are missing in the core of the fiber. The refractive index $n(\lambda)$ of As_2Se_3 is determined in terms of Sellemier formula[14]

$$n(\lambda) = \sqrt{1 + \lambda^2 \left(\frac{A_0^2}{\lambda^2 - A_1^2} + \frac{A_2^2}{\lambda^2 - 19} + \frac{A_3^2}{\lambda^2 - 4A_1^2} \right)}, \tag{1}$$

where A_0=2.234921, A_1=0.24164, A_2=0.347441, A_3=1.308575, and λ is the wavelength (in units of micron). By changing the pitch ratio $\eta = \Lambda_y/\Lambda_x$, where Λ_x (Λ_y) is the pitch along the x (y) axis. The structural symmetry can be broken, which leads to another important modal property, known as birefringence. In the triangular arrangement, air holes are placed in concentric rings around the core. Since the influence of the air holes in the innermost ring is dominant, to further enhance the birefringence, modification of air-hole diameters in this ring will be more effective.[18–20] The air-hole diameters (d_1, d_2, d_3, and d_4) in the innermost cladding decrease proportionally upward and downward along the y axis. The parameters in the other cladding are defined as d_0. We set $\eta = 1.25$, $\Lambda = \Lambda_x$, $d_0/\Lambda = 0.8$, $d_1/\Lambda = 0.8$, $d_2/\Lambda = 0.6$, $d_3/\Lambda = 0.4$, and $d_4/\Lambda = 0.2$ as constant parameters and analyse the mode by using the CUDOS MOF utilities. The fundamental mode field distribution is absolutely limited in the core so that the mode-limited loss substantially decreases.

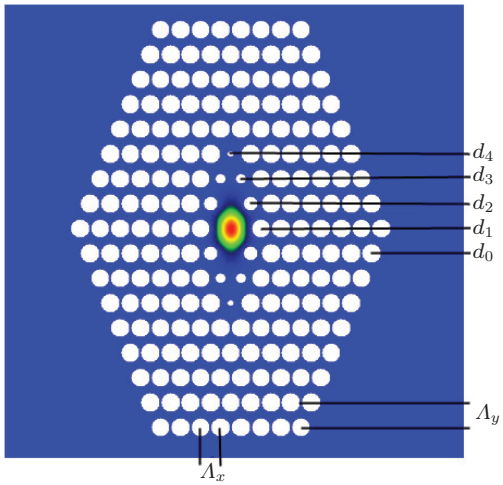


Fig. 1. (colour online) Cross-sectional structure and fundamental mode field distribution of the As_2Se_3 PCF.

2.1. High birefringence

Due to its asymmetric structure, the PCF can keep in a specific input polarization state, and the corresponding birefringence is expected to be high. Birefringence is an important parameter for scaling the performance of polarization-maintained optical fibers. It can be expressed as

$$B = \left| \mathrm{Re}\left(n_{\mathrm{eff},x}\right) - \mathrm{Re}\left(n_{\mathrm{eff},y}\right) \right|, \tag{2}$$

where $n_{\mathrm{eff},x}$ and $n_{\mathrm{eff},y}$ represent the effective index of the x- and y-polarized modes, respectively. Re(·) represents the real part. Figure 2 shows the dependence of birefringence B on the air-hole pitch Λ. B increases with the increase of wavelength but decreases with the increase of pitch Λ, which is consistent with other literatures. In our proposed design, we achieve a high birefringence of $B = 0.24601969 \times 10^{-2}$ at $\lambda = 4$ μm and $\Lambda = 2$ μm, which is a little smaller than those in Refs. [21] and [22] and can keep the polarization state along the propagation direction.

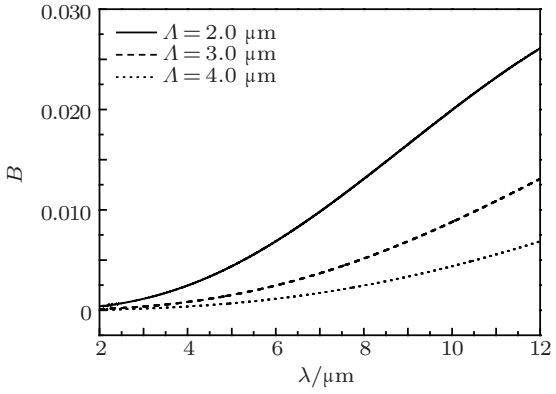


Fig. 2. Birefringence versus wavelength in a range of 2–12 μm when air-hole pitch $\Lambda = 2.0$ μm (solid line), 3.0 μm (dashed line), and 4.0 μm (dotted line), respectively.

2.2. Polarization extinction ratio

The polarization extinction ratio ($R_{\rm pe}$) is another key parameter for a polarization-maintained fiber. When only one linearly polarized mode HE_{11}^{x} is launched in the incident port of the fiber, due to the coupling effect, another orthogonally polarized mode HE_{11}^{y} is also slightly stimulated. Namely, an incident linearly polarized light becomes an elliptically polarized light, and the field intensities along the long and short axes are $E_{\max}$ and $E_{\min}$, respectively. Thus, $R_{\rm pe}$ is used to reflect the polarization-maintaining extent of the fibers. It can be expressed by

$$R_{\rm pe} = 10 \times \log\left(\frac{1+d_{\rm p}}{1-d_{\rm p}}\right) = 10 \times \log\left(\frac{E_{\max}^2}{E_{\min}^2}\right), \quad (3)$$

where $d_{\rm p}$ is the degree of polarization. $E_{\max}$ and $E_{\min}$ are calculated with a three-dimensional full-vector finite-difference beam propagation method. Simulation results show that $R_{\rm pe} = 30.22738$ for $\Lambda = 2.0$ μm, which is not high but meets a polarization-maintained requirement.

2.3. Dispersion properties

Chromatic dispersion is a phenomenon that inevitably produces signal distortion in the process of transmission. Fiber dispersion depends on the propagation constant and refractive index of materials, leading to the waveguide dispersion $D_{\rm w}(\lambda)$ and material dispersion $D_{\rm m}(\lambda)$. Thus, we obtain

$$D(\lambda) = D_{\rm w}(\lambda) + D_{\rm m}(\lambda), \quad (4)$$

$$D_{\rm w}(\lambda) = -\frac{\lambda}{c}\frac{{\rm d}^2 n_{\rm eff}(\lambda)}{{\rm d}\lambda^2}, \quad (5)$$

$$D_{\rm m}(\lambda) = -\frac{\lambda}{c}\frac{{\rm d}^2 n(\lambda)}{{\rm d}\lambda^2}, \quad (6)$$

where $n_{\rm eff}(\lambda)$ represents the effective index of guided mode and can be calculated with the CUDOS utilities, $n(\lambda)$ can be obtained with the scaling law (Eq. (1)), c is the velocity of light in vacuum. The group-velocity dispersion β_2 is commonly used in place of the dispersion parameter D, which can be expressed as follows:

$$D(\lambda) = \frac{{\rm d}\beta_1}{{\rm d}\lambda} = -\frac{2\pi c}{\lambda^2}\beta_2. \quad (7)$$

Figure 3 shows the chromatic dispersion for the x- and y-polarized fundamental modes in a wavelength range of 2–12 μm for $\Lambda = 2.0$ μm, 3.0 μm, and 4.0 μm. The zero dispersion wavelengths (ZDWs) along the x (y) axis are 3.62 (3.77), 4.25 (4.38), and 4.77 (4.89) μm for $\Lambda = 2.0$, 3.0, and 4.0 μm, respectively. As the pitch increases, the anomalous dispersion region begins at a longer wavelength.

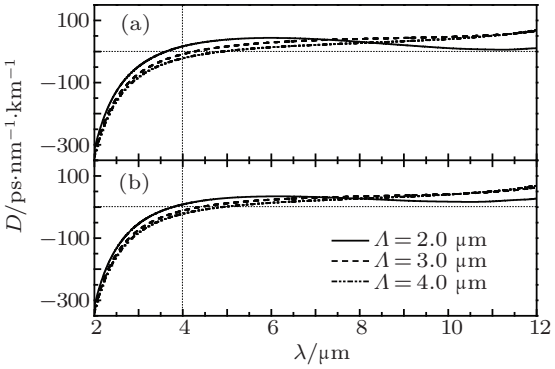


Fig. 3. Chromatic dispersion for the (a) x and (b) y axes in a wavelength range of 2–12 μm for $\Lambda = 2.0$, 3.0, and 4.0 μm, respectively.

2.4. Highly nonliear coefficient

Due to the combination of the highly nonlinear refractive index n_2 of chalcogenide glasses and the strong mode confinement of PCFs, chalcogenide glass PCFs are used as suitable nonlinear media, which allow strong nonlinear effects. The nonlinear effect is scaled by the nonlinear coefficient γ, which can be calculated as follows:

$$\gamma(\lambda) = \frac{2\pi n_2}{\lambda A_{\rm eff}}, \quad (8)$$

where n_2 equals 2.4×10^{-17} m^2/W for As_2Se_3.[14] $A_{\rm eff}$ is the effective mode field area, which can be expressed as

$$A_{\rm eff} = \frac{(\int\int_{-\infty}^{\infty} |F(x,y)|^2 {\rm d}x{\rm d}y)^2}{(\int\int_{-\infty}^{\infty} |F(x,y)|^4 {\rm d}x{\rm d}y)}, \quad (9)$$

where $F(x,y)$ is the distribution of the fundamental mode field.

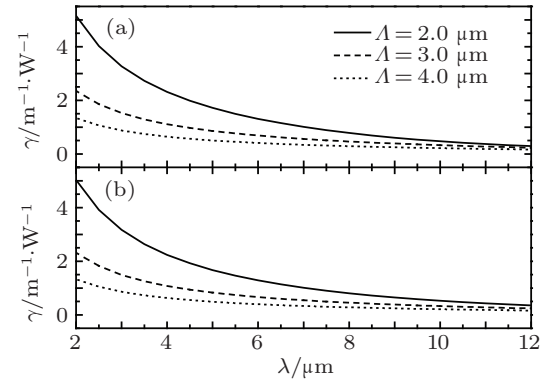


Fig. 4. Nonlinear coefficient for the (a) x and (b) y axes versus wavelength for $\Lambda = 2.0$, 3.0, and 4.0 μm, respectively.

Figure 4 shows the nonlinear coefficient as a function of wavelength for the x and y axes when air-hole

pitch Λ = 2.0, 3.0, and 4.0 μm, respectively. The nonlinear coefficient γ decreases with the increase of wavelength but increases with the decrease of pitch Λ. In the case of λ = 4 μm, the values of γ for the x (y) axis are 2.310 (2.237), 1.109 (1.077), and 0.6438 (0.6285) $\mathrm{m}^{-1}\cdot\ \mathrm{W}^{-1}$ for Λ = 2.0, 3.0, and 4.0 μm, respectively.

3. Broadband polarized SCG

In high birefringence PCFs, optical pulse propagation can be viewed as propagations of two polarized pulse in optical fiber. Assuming that the angle between the polarization state of the incident pulse and the x axis is θ, the slowly varying polarization amplitudes A_x and A_y satisfy the following coupled nonlinear Schrödinger equations (CNLSE):[23]

$$\begin{aligned}&\frac{\partial A_x}{\partial z}+\sum_{n\geq 2}\beta_{nx}\frac{\mathrm{i}^{n-1}}{n!}\frac{\partial^n A_x}{\partial T^n}\\&=\mathrm{i}\gamma_x\bigg(|A_x|^2A_x+\frac{2}{3}|A_y|^2A_x\\&\quad+\frac{\mathrm{i}}{\omega_0}\frac{\partial(|A_x|^2)A_x}{\partial T}-T_{\mathrm{R}}A_x\frac{\partial|A_x|^2}{\partial T}\bigg),\end{aligned}\tag{10}$$

$$\begin{aligned}&\frac{\partial A_y}{\partial z}+d\frac{\partial A_y}{\partial T}+\sum_{n\geq 2}\beta_{ny}\frac{\mathrm{i}^{n-1}}{n!}\frac{\partial^n A_y}{\partial T^n}\\&=\mathrm{i}\gamma_y\bigg(|A_y|^2A_y+\frac{2}{3}|A_x|^2A_y\\&\quad+\frac{\mathrm{i}}{\omega_0}\frac{\partial(|A_y|^2)A_y}{\partial T}-T_{\mathrm{R}}A_y\frac{\partial|A_y|^2}{\partial T}\bigg),\end{aligned}\tag{11}$$

where T is the time in a reference frame moving at the group velocity along the x axis ($T=t-z/v_{\mathrm{g}}\equiv t-\beta_{1x}z$), $\beta_{nj}\,(j=x,y)=\partial^n\beta_j/\partial\omega^n\,|_{\omega_0}$ is the nth term of Taylor series for the propagation constant $\beta_n(\omega)$ at the center frequency ω_0, γ_j can be calculated according to Eq. (8), and $d=1/v_{\mathrm{g}x}-1/v_{\mathrm{g}y}=\beta_{1x}-\beta_{1y}$ is the walk-off parameter. The characteristic Raman time is defined as the first moment of the nonlinear response function

$$T_{\mathrm{R}}\equiv\int_0^\infty t\cdot R(t)\mathrm{d}t\approx f_{\mathrm{R}}\int_0^\infty t\cdot h_{\mathrm{R}}(t)\mathrm{d}t,\tag{12}$$

where $f_{\mathrm{R}}=0.115$ and

$$h_{\mathrm{R}}(t)=\frac{\tau_1^2+\tau_2^2}{\tau_1\tau_1^2}\exp\left(-\frac{t}{\tau_2}\right)\cdot\sin\left(-\frac{t}{\tau_1}\right),$$

with τ_1 = 23.1 fs and τ_2 = 195 fs for chalcogenide glasses.[14]

Next, we analyse the SCG in the proposed birefringent PCFs. The pumping wavelength plays an important role in the SCG dynamics and therefore needs to be carefully chosen. It is clear from Fig. 3 that the ZDWs for our proposed fibers are close to 4 μm. Therefore, we use a mid-IR optical parametric oscillator, which is synchronously pumped by an erbium-doped fiber laser, as the pump pulse in order to generate a broad continuum in the mid-IR region. Specifically, a Gaussian idler with a maximum average power of 37 mW, a repetition rate of 90 MHz, a pulse length of 480 fs, and a central wavelength of 4.0 μm is produced.[24]

Table 1. Taylor series for propagation constant $\beta_n(\omega)$ at the center wavelength of 4.0 μm for Λ = 2.0, 3.0, and 4.0 μm, respectively.

$\beta_n(\omega)/\mathrm{s}^{\mathrm{n}}\cdot\mathrm{m}^{-1}$	Λ=2.0 μm		Λ=3.0 μm		Λ=4.0 μm	
	x axis	y axis	x axis	y axis	x axis	y axis
β_1	0.1872×10^{-7}	0.1871×10^{-7}	0.1865×10^{-7}	0.1865×10^{-7}	0.1863×10^{-7}	0.1862×10^{-7}
β_2	-0.1443×10^{-24}	-0.7427×10^{-25}	0.7093×10^{-25}	0.9812×10^{-25}	0.1695×10^{-24}	0.1824×10^{-24}
β_3	0.3186×10^{-38}	0.2663×10^{-38}	0.2239×10^{-38}	0.2043×10^{-38}	0.1716×10^{-38}	0.1625×10^{-38}
β_4	-0.9342×10^{-53}	-0.9627×10^{-53}	-0.1174×10^{-52}	-0.1004×10^{-52}	0.8583×10^{-53}	-0.7497×10^{-53}
β_5	0.3043×10^{-67}	0.1508×10^{-66}	0.2174×10^{-66}	0.1978×10^{-66}	0.2021×10^{-66}	0.1809×10^{-66}
β_6	-0.7029×10^{-80}	-0.2480×10^{-80}	-0.1637×10^{-80}	-0.1287×10^{-80}	-0.1171×10^{-80}	-0.1190×10^{-80}
β_7	0.1022×10^{-93}	-0.1151×10^{-93}	-0.1194×10^{-93}	-0.1262×10^{-93}	-0.1350×10^{-93}	-0.1252×10^{-93}
β_8	0.9358×10^{-107}	0.4811×10^{-107}	0.1895×10^{-107}	0.1811×10^{-107}	0.1565×10^{-107}	0.1734×10^{-107}
β_9	-0.2526×10^{-120}	0.7169×10^{-121}	0.1342×10^{-120}	0.1434×10^{-120}	0.1598×10^{-120}	0.1453×10^{-120}
β_{10}	-0.8128×10^{-134}	-0.6613×10^{-134}	-0.4503×10^{-134}	-0.4498×10^{-134}	-0.4509×10^{-134}	-0.4517×10^{-134}
β_{11}	0.4007×10^{-147}	0.2296×10^{-148}	-0.5698×10^{-148}	-0.7036×10^{-148}	-0.8406×10^{-148}	-0.7100×10^{-148}
β_{12}	0.2564×10^{-161}	0.6744×10^{-161}	0.5499×10^{-161}	0.5755×10^{-161}	0.5876×10^{-161}	0.5708×10^{-161}
β_{13}	-0.4611×10^{-174}	-0.1702×10^{-174}	-0.7272×10^{-175}	-0.6295×10^{-175}	-0.5012×10^{-175}	-0.6021×10^{-175}
β_{14}	0.7806×10^{-188}	-0.1716×10^{-188}	-0.2540×10^{-188}	-0.3026×10^{-188}	-0.3435×10^{-188}	-0.3110×10^{-188}
β_{15}	0.1826×10^{-201}	0.1724×10^{-201}	0.1191×10^{-201}	0.1234×10^{-201}	0.1241×10^{-201}	0.1250×10^{-201}

Based on the above results, the CNLSE is solved numerically by using the adaptive split-step Fourier method implemented in Fortran.[26] In addition, corresponding $\beta_n(\omega)$ is computed up to the 15th and listed in Table 1.

It is well known that the pulse can be broadened in PCFs because of the interplay between nonlinear effects. The mechanism of pulse broadening by ultrashort pulses in PCFs strongly depends on the difference between the pump wavelength and the ZDW. In what follows, the pump wavelength is tuned in different dispersion regions of fibers by tuning the air-hole pitch so that the extent and mechanism of pulse broadening are markedly different.

For a PCF with $\Lambda = 2.0$ μm, a wavelength of 4 μm is located in an anomalous dispersion region near ZDW. Figure 5 shows the simulated spectrograms when the wave propagates along the PCF at $\Lambda = 2.0$ μm, where the average pump power is tuned to the maximum ($P_{\rm av} = 37$ mW). From Fig. 5, we can see that the pulse is broadened symmetrically in the range of $0 < L < 0.3$ cm due to self-phase modulation (SPM) and cross-phase modulation (XPM). Then, the mid-IR broadband supercontinuum is generated for a longer propagation length. The width of the SCG is up to 12 μm. This can be explained as follows: since the second-order dispersion of the fiber is negative and small, the higher-order solitons are formed by the combined effects of group velocity dispersion (GVD), higher-order dispersion (HOD), stimulated Raman scattering (SRS), self-steepening effect, and so on, which leads to splitting. Moreover, the phenomenon of splitting is more and more obvious. Compared with the spectrum in the x-polarized direction, the spectrum in the y-polarized direction is wider since ZDW in the y axis is closer to the central wavelength of 4 μm.

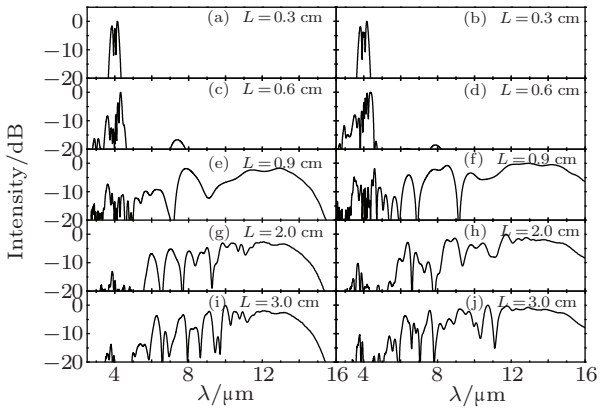


Fig. 5. Spectral evolution of the input pulse at $\Lambda = 2.0$ μm after a propagation distance of (a), (b) 0.3, (c), (d) 0.6, (e), (f) 0.9, (g), (h) 2.0, and (i), (j) 3.0 cm . The left and right columns correspond to the cases of the x axis (0°) and y axis (90°), respectively.

For a PCF with $\Lambda = 3.0$ μm, the wavelength of 4 μm is located in the normal dispersion region near ZDW. Figure 6 shows the simulated spectrograms as the wave propagates along the PCF when $\Lambda = 3.0$ μm, where the average pump power is tuned to the maximum ($P_{\rm av} = 37$ mW). From Fig. 6, we can see that the pulse is greatly broadened and supercontinuum is finally generated when the transmission distance $L = 3$ cm. It can be explained as follows: in the initial stage, the spectral broadening results mainly from the SPM; in the later stage, the blue-shifted components of spectrum gradually enter the normal dispersion region, and the red-shifted components enter the anomalous dispersion region and then are broadened in depth, which is due to the spectral broadening mechanism for anomalous dispersion region. In addition, in other equivalent conditions, the supercontinuum is narrower in the normal dispersion region than in the anomalous dispersion region. The spectrum in the x-polarized direction is wider than that in the y-polarized direction due to a similar reason that the ZDW in the x axis is closer to the central wavelength of 4 μm.

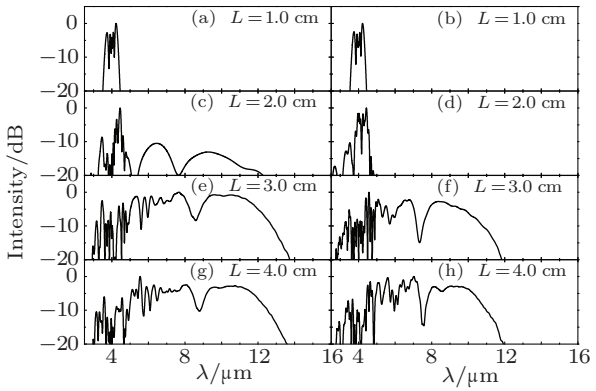


Fig. 6. Spectral evolution of the input pulse at $\Lambda = 3.0$ μm after a propagation distance of (a), (b) 1.0, (c), (d) 2.0, (e), (f) 3.0, and (g), (h) 4.0 cm. The left and right columns correspond to the cases of the x axis (0°) and y axis (90°), respectively.

For a PCF with $\Lambda = 4.0$ μm, the wavelength of 4 μm is located in the normal dispersion region away from ZDW. Figure 7 shows the simulated spectrograms as the wave propagates along a PCF when $\Lambda = 4.0$ μm, where the average pump power is tuned to the maximum ($P_{\rm av} = 37$ mW). The results indicate that the phenomenon of optical wave breaking occurs in a short distance. In the case of normal dispersion region, the GVD and SPM can induce chirp

through the entire pulse. Because of the nonlinear nature of the composite chirp, different parts of the pulse propagate at different speeds. In particular, in the case of normal dispersion region, the red-shifted part on the leading edge travels faster and surpasses the unshifted part in the forward tail of the pulse. The opposite situation occurs for the blue-shifted part on the trailing edge. In both cases, the leading and trailing parts of the pulse contain two interfered lights at different frequencies. Finally, the phenomenon of optical wave breaking emerges. As the distance increases, the spectrum becomes asymmetric due to HOD and SRS. However, the spectral broadening is limited finally because the rapid broadening of the pulse in the time domain results in the significant decrease of the peak power of the pulse.

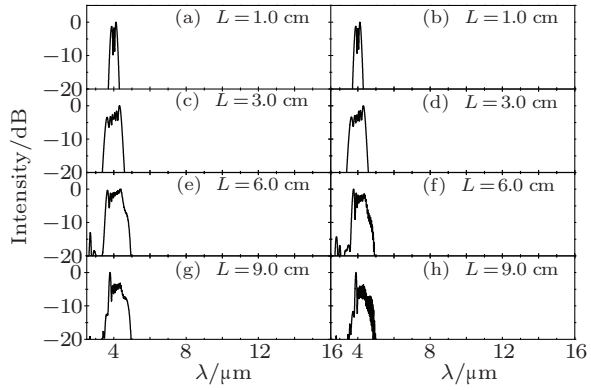


Fig. 7. Spectral evolution of the input pulse at $\Lambda = 4.0$ μm after a propagation distance of (a), (b) 1.0, (c), (d) 3.0, (e), (f) 6.0, and (g), (h) 9.0 cm. The left and right columns correspond to the cases of the x axis (0°) and y axis (90°), respectively.

Figure 8 shows the simulated spectrograms for different air-hole pitches, where the average pump power $P_{\rm av} = 37$ mW and the transmission distance $L = 3$ cm. For $\Lambda = 2.0$ μm, the spectrograms in the x and y axes are both broadened to a longer wavelength, but have gaps at the wavelength of about 4.2 μm. For $\Lambda = 3.0$ μm, the spectrograms in the x and y axes are both broadened to a shorter wavelength. For $\Lambda = 4.0$ μm, the widths of the spectrograms in the x and y axes are the narrowest.

As stated above, the air-hole pitches have a tremendous influence on spectrograms. However, since errors of air-hole pitches are inevitable in the actual drawing process, it is necessary to consider the impact of the pitch-tolerance on the spectral broadening. Figure 9 shows the simulated spectrograms for different air-hole pitches, where the average pump power $P_{\rm av} = 37$ mW and the transmission distance $L = 3$ cm. It can be seen that the widths of the broadened spectrograms in the x and y axes reach up to 12 μm. Small peaks can be found at a wavelength of less than 4.0 μm, and the tendency of the spectrum splitting is the same in a wavelength range of 4.0–12.0 μm.

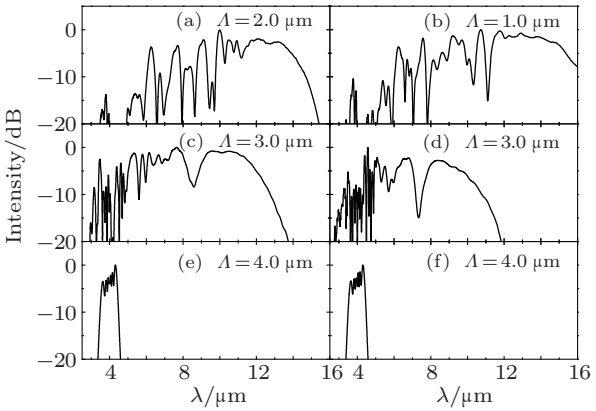


Fig. 8. Spectral evolution of the input pulse for an air-hole pitch of (a), (b) 2.0, (c), (d) 3.0, and (e), (f) 4.0 μm, respectively. $P_{\rm av} = 37$ mW and $L = 3$ cm. The left and right columns correspond to the cases of the x axis (0°) and y axis (90°), respectively.

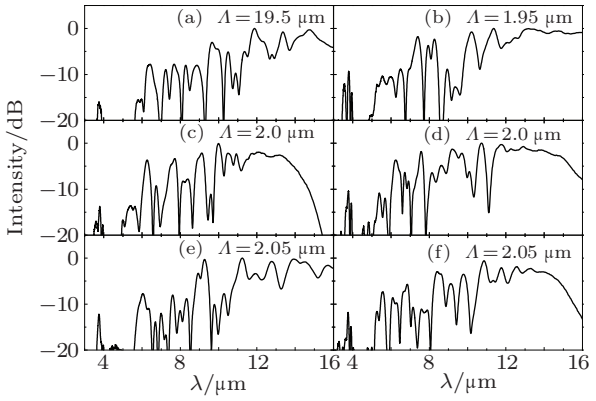


Fig. 9. Spectral evolution of the input pulse under the impact of the pitch tolerance (a), (b) $\Lambda = 1.95$ μm, (c), (d) $\Lambda = 2.0$ μm, and (e), (f) $\Lambda = 2.05$ μm, respectively. The left and right columns correspond to the cases of the x axis (0°) and y axis 90°, respectively.

To highlight the polarization properties, it is a good way to check if the interaction actually occurs by simulating the SCG in the x and y axes (0° and 90°) separately under the condition that the average power is only half of its maximum value. In Fig. 10, taking $\Lambda = 2$ μm for example, the above four charts represent different alignment conditions at the maximum average power ($P_{\rm av} = 37$ mW), the below two charts represent the x axis (0°) and y axis (90°) when $P_{\rm av} = 18.5$ mW. It shows that the spectrum at 0° (90°) when $P_{\rm av} = 18.5$ mW exactly matches its corresponding x- (y)-polarized components at 45° when $P_{\rm av} = 37$ mW. The results can serve as a strong proof

that there are no interactions between the x-polarized components and y-polarized components at 45° and no couplings either.

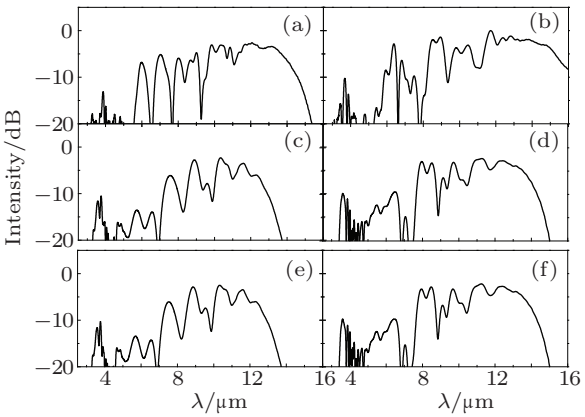


Fig. 10. Spectral evolution of the input pulse at the maximum average power and its half value at $\Lambda = 2.0$ μm. Maximum average power ($P_{\rm av} = 37$ mW): (a) x axis (0°), (b) y axis (90°), (c) x-axis components at 45°, (d) y-axis components at 45°; its half value ($P_{\rm av} = 18.5$ mW): (e) x axis (0°), (f) y axis (90°).

However, in practical experiments or applications, the input pump pulses may not be precisely aligned along the principal axis. Therefore, we additionally consider the alignment error by choosing pump alignments of 2° and 92° for a 3-cm PCF with a pitch of 2 μm, as shown in Fig. 11. The pump wavelength, input pulse format and duration are the same as above. It can be seen that when the input pulse is linearly polarized along the x (y) axis, the supercontinuum is mainly x- (y-)polarized. Thus, the polarization state can be well kept in our optimal PCF.

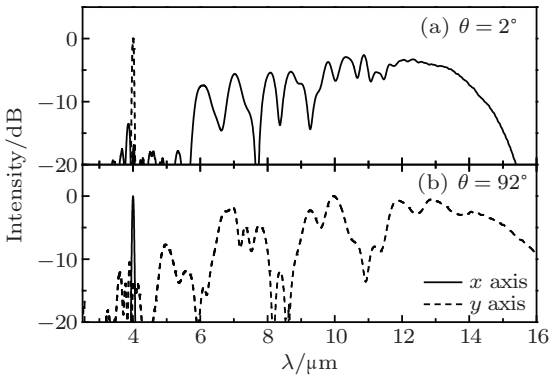


Fig. 11. When $\Lambda = 2$ μm, spectral evolution of the input pulse at (a) $\theta = 2°$ and (b) $\theta = 92°$ after the PCF propagation.

4. Conclusion

A simple novel type of PCF for mid-IR supercontinuum is proposed: a non-equilateral triangular lattice As_2Se_3 chalcogenide PCF with four missing air holes in the core and different-diameter air holes in the innermost cladding. The PCF provides high birefringence, high polarization extinction ratio, considerable chromatic dispersion, and high nonlinearity through properly tuning air-hole pitches, of which ZDW is about 4 μm. We use an idler with a maximum average power of 37 mW, repetition rate of 90 MHz, a pulse length of 480 fs, and a central wavelength of 4.0 μm as the input pump pulse to investigate its transmission. The pump wavelength is located in different dispersion regions of the fibers for different air-hole pitches, so that the extent and mechanism of pulse broadening are remarkably different. It is worth mentioning that the mid-IR broadband polarized supercontinuum has been obtained in a 3-cm PCF with an optimal pitch of 2 μm. The width of the supercontinuum reaches up to 12 μm at −20 dB. Such a supercontinuum can be widely applied in basic science, industry, communications, medical treatment, and the military field. In addition, it is found that no coupling between orthogonal eigenpolarization modes is observed when the average power is 37 mW and the polarization state can be well maintained.

References

[1] Holzwarth R, Udem T, Hänsch T W, Knight J C, Wadsworth W J and Russell P S J 2000 *Phys. Rev. Lett.* **85** 2264

[2] Hartl I, Li X D, Chudoba C, Ghanta R K, Ko T H, Fujimoto J G, Ranka J K and Windeler R S 2001 *Opt. Lett.* **26** 608

[3] Xia C, Kumar M, Kulkarni O P, Islam M N, Terry J F L, Freeman M J, Poulain M and Mazé G 2006 *Opt. Lett.* **31** 2553

[4] Qin G, Yan X, Kito C, Liao M, Chaudhari C, Suzuki T and Ohishi Y 2009 *Appl. Phys. Lett.* **95** 161103

[5] Price J H V, Monro T M, Ebendorff-Heidepriem H, Poletti F, Horak P, Finazzi V, Leong J Y Y, Petropoulos P, Flanagan J C, Brambilla G, Xian F and Richardson D J 2007 *IEEE J. Sel. Top. Quantum Electron.* **13** 738

[6] Feng X, Loh W H, Flanagan J C, Camerlingo A, Dasgupta S, Petropoulos P, Horak P, Frampton K E, White N M, Price J H, Rutt H N and Richardson D J 2008 *Opt. Express* **16** 13651

[7] Liao M, Chaudhari C, Qin G, Yan X, Suzuki T and Ohishi Y 2009 *Opt. Express* **17** 12174

[8] Domachuk P, Wolchover N A, Cronin-Golomb M, Wang A, George A K, Cordeiro C M B, Knight J C and Omenetto F G 2008 *Opt. Express* **16** 7161

[9] Lamont M R, Luther-Davies B, Choi D Y, Madden S and Eggleton B J 2008 *Opt. Express* **16** 14938

[10] Yeom D I, Mägi E C, Lamont M R E, Roelens M A F, Fu L and Eggleton B J 2008 *Opt. Lett.* **33** 660

[11] Brandon S, Peter T, Fred K, Vinh N, Jas S and Ishwar A 2005 *A*dvanced Solid-State Photonics Vienna, Austria, February 6–9, 2005 TuC5
[12] Hu J, Menyuk C R, Shaw L B, Sanghera J S and Aggarwal I D 2010 *Opt. Express* **18** 6722
[13] Weiblen R J, Docherty A, Hu J and Menyuk C R 2010 *Opt. Express* **18** 26666
[14] Ung B and Skorobogatiy M 2010 *Opt. Express* **18** 8647
[15] Zhu Z and Brown T G 2004 *J. Opt. Soc. Am.* B **21** 249
[16] Martins E R, Spadoti D H, Romero M A and Borges B H V 2007 *Opt. Express* **15** 14335
[17] Proulx A, Ménard J M, Hô N, Laniel J M, Vallée R and Paré C 2003 *Opt. Express* **11** 3338
[18] Dabas B and Sinha R K 2011 *Opt. Commun.* **284** 1186
[19] Yan F P, Li Y F, Wang L, Gong T R, Liu P, Liu Y, Tao P L, Qu M X and Jian S S 2008 *Acta Phys. Sin.* **57** 5735 (in Chinese)
[20] Yan F P, Wang L, Mao X Q, Gong T R, Liu P, Tao P L and Peng W J 2010 *Opt. Commun.* **283** 3658
[21] Xia C M, Zhou G Y, Han Y, Liu Z L and Hou L T 2011 *Acta Phys. Sin.* **60** 094213 (in Chinese)
[22] Wang X Y, Li S G, Liu S, Zhang L, Yin G B and Feng R P 2011 *Acta Phys. Sin.* **60** 064213 (in Chinese)
[23] Agrawal G P 2010 *Nonlinear Fiber Optics and Its Applications* 2nd edn., translated by Jia D F and Yu Z H (Beijing: Publishing House of Electronics Industry) pp. 29–32
[24] Agrawal G P 2010 *Applications of Nonlinear Fiber Optics* (2nd ed.) (California: Academic Press) pp. 135–139
[25] Haakestad M W, Fonnum H, Arisholm G, Lippert E and Stenersen K 2010 *Opt. Express* **18** 25379
[26] Li S G, Xing G L, Zhou G Y, Han Y, Hou L T, Hu M L, Li Y F and Wang Q Y 2006 *Chin. Phys.* **15** 437